Sperm gatekeeping: 3D imaging reveals a constricted entrance to zebra finch sperm storage tubules

Authors: T. Mendonca, A. J. Cadby and N. Hemmings

Short Title: Sperm gatekeeping

Abstract:

Females across many internally fertilising taxa store sperm, often in specialised storage organs in their reproductive tracts. In birds, several hundred sperm storage tubules exist in the utero-vaginal junction of the oviduct and there is growing evidence that sperm storage in these tubules is selective. The mechanisms underlying female sperm storage in birds remain unknown due to our limited ability to make three dimensional, live observations inside the large, muscular avian oviduct. Here, we describe a new application of fluorescence selective plane illumination microscopy to optically section oviduct tissue from zebra finch *Taeniopygia guttata* females label-free, by harnessing tissue autofluorescence. Our data provide the first description of the 3D structure of sperm storage organs in any vertebrate and reveal the presence of gate-like constricted openings that may play a role in sperm selection.

Statement of Significance:

Female birds can store sperm in microscopic tubular structures in their reproductive tract for up to several months, depending on species. Studying these sperm storage tubules has been a major challenge due to the muscular and opaque nature of reproductive tracts in birds. We have developed a new method for imaging live reproductive tract tissue using selective plane illumination microscopy, a fluorescence microscopy technique. From these images, we could extract three-dimensional measurements of sperm storage tubules and found these structures to have a gate-like constriction, providing evidence that females can actively select sperm at storage and ultimately influence the paternity of her offspring. Understanding these reproductive adaptations can help improve captive breeding programs and similar conservation strategies.

Introduction:

Across many internal fertilisers, females have evolved the capacity to maintain viable sperm in specialised sperm storage organs in their reproductive tract as a strategy to maximise fertility. Sperm storage ensures the female has sufficient sperm for fertilisation when copulation and ovulation are not synchronised (1). Since female promiscuity is common across taxa (e.g. birds (2), mammals (3–5), reptiles (6), fishes (7) and insects (8–10)), storage also provides the opportunity for females to exert control over post-copulatory processes (11–13). Post-copulatory sexual selection has driven the diversification of sperm storage organs, which vary from single bean-shaped structures in damselflies (14, 15) or one or more sac-like spermathecae in certain fly species (16) (17), to multiple epithelial crypts in snakes (18), lizards (19), turtles (20) and birds (21, 22).

In birds, epithelial sperm storage crypts are called sperm storage tubules (SSTs) and are located in the utero-vaginal junction (UVJ) of the oviduct (23). The number of SSTs possessed by a single female ranges from around 500 in the budgerigar (*Melopsittam undulates*) to 20,000 in the turkey (*Meleagris gallopavo*) (24). A growing body of evidence suggests that avian SSTs are an important site of sperm selection. Steele and Wishart (25) experimentally demonstrated that chicken (*Gallus domesticus*) sperm without surface membrane proteins could not enter the SSTs after normal intra-vaginal artificial insemination, even though these sperm were capable of fertilising the ovum when inseminated beyond the vagina and UVJ. Bobr *et al.* (23) also noted a lack of abnormal sperm in chicken SSTs, suggesting that abnormal sperm are unable to reach or enter sperm storage sites. The large number of SSTs present in the avian oviduct may

also allow spatio-temporal segregation of sperm from competing ejaculates (26–28).

Despite evidence that SSTs may act as a filter for high quality sperm, the mechanisms by which sperm are selected at the time of storage remain poorly understood, and how sperm enter and exit the SSTs is unknown. Froman (29) proposed a model where sperm motility, rather than SST function, is pivotal in sperm retention in SSTs. According to this model, sperm must maintain an optimum swimming velocity to maintain their position and counter a fluid current within the SST. This model was supported by evidence that faster sperm emerged out of SSTs later than slower sperm (30), and that passive loss of sperm from storage might be sufficient to explain last male precedence in the domestic fowl, turkeys, and zebra finches (*Taeniopygia guttata*) [31,32; but see 27]. However, there have been no published observations of sperm swimming inside the SSTs, and our own unpublished observations suggest sperm are not motile in storage (see Supplementary Material). Several studies have detected the presence of sperm motility suppressors such as lactic acid in Japanese quail (*Coturnix japonica*) SSTs (33), calcium and zinc in the SSTs of chicken, turkeys and Japanese quail (34, 35), and carbonic anhydrase in the SSTs of turkeys, common quail (*Coturnix coturnix*) and ostriches (*Struthio camelus*) (36–38), and the neurotransmitter acetylcholine, released by nerve endings detected in the vicinity of SSTs (39), has been shown to enhance sperm motility (40), implying a nervous control on sperm mobilisation at ejection from SSTs. Additionally, Hiyama *et al.* (41) presented evidence for the potential role of heat shock protein 70 (HSP70) (42) in enhancing sperm motility at the point of sperm release. The presence of such sperm motility suppressors and activators within or near the SSTs suggests that release of sperm from storage may not be as passive as Froman (29) suggested.

Rather than acting as passive refugia, SSTs may instead be dynamic structures, capable of active constriction and dilation to mediate the entrance and exit of sperm. Although numerous studies have failed to find smooth muscle fibres or myoepithelial cells (39, 43, 44) around SSTs, Freedman *et al.* (39) detected fibroblast-like cells and an F-actin rich cytoskeletal mesh called the "terminal web" in turkey SST epithelia. The terminal web is composed of contractile proteins (actin and myosin) and has been shown to contribute to contractility in other tissues, such as intestinal brush border cells (45, 46) and embryonic pigmented epithelia in chickens (47). Freedman *et al.* (39) also found terminal innervations in the turkey UVJ, suggesting there may be some degree of nervous control over SST function. Recent evidence also suggests the possibility of SST contraction, influenced hormonally by the action of progesterone (48, 49). It is therefore possible that the passage of sperm into and out of storage is controlled, to some degree, by the physical structure of SSTs themselves.

Our understanding of how SST structure influences sperm storage is limited by our relatively basic knowledge of SST morphology. The avian oviduct is convoluted, with opaque, muscular walls, creating numerous practical limitations for making observations of tubules in living epithelial tissue using conventional microscopy techniques. Empirical studies of SST morphology have so far used histology (23, 50, 51) and electron microscopy (34, 43, 52) on fixed tissue sections, but these approaches not only remove functional information, but typically provide two-dimensional information only. Moreover, serial sectioning is laborious, and loss of material can be difficult to avoid. Commonly used light microscopy techniques rely on thin sections and squash

preparations (26, 53), which are inappropriate for large tissue samples since they distort structures of interest and allow only limited imaging depths.

In this study we developed a novel method for live, *ex vivo* 3D imaging of SST structure using selective plane illumination microscopy (SPIM). SPIM is highly suitable for imaging large samples at cellular resolution and has lower phototoxicity levels than with other optical sectioning methods which makes it a viable option for imaging living tissue (54, 55). Using SPIM, we were able to optically section UVJ mucosal tissue up to depths of 100 μm without distorting or damaging their structure. We provide the first quantitative estimates of the 3D structure of sperm storage tubules in living tissue, including the relationship between SST length and diameter, and report the existence of a previously undescribed gate-like constriction at the entrance to tubules that may act to regulate sperm transport into and out of storage.

Materials and Methods:

Animals

This study was approved by the University of Sheffield, UK. All procedures performed conform to the legal requirements for animal research in the UK and were conducted under a project licence (PPL 40/3481) issued by the Home Office.

Zebra finches were from a captive population kept at the University of Sheffield (56, 57). Females (all between one to three years old) were placed in unisex housing for at least two weeks before being paired with males, in double-cages (dimensions of each individual cage: 0.6m x 0.5m x 0.4m) separated by a wire-mesh with the male

and female on either side. Each double-cage had a modified nest-box, also with a wire-mesh partition, to allow both birds to enter the nest. This set up allowed the male and female to establish a normal breeding pair bond and enter breeding condition, while preventing them from copulating and therefore ensuring the female had no sperm in her SSTs (sperm can be stored for up to 12 days after mating in zebra finches (24)). Females were only included in the study once they had started to lay eggs, to ensure their oviduct was in full reproductive condition. After they laid their second egg, females were euthanized (in accordance with Schedule 1 [Animals (Scientific Procedures) Act 1986)] and dissected immediately.

Sample preparation

The oviduct, including the cloaca, was immediately removed from the female and the connective tissue surrounding it was cleared to uncoil and straighten the vagina and the UVJ. The lower end of the oviduct was cut through the middle of the uterus to obtain a segment that included the UVJ, vagina and cloaca. This piece of the oviduct was then cut open lengthwise and pinned flat on a petri-dish filled with silicone elastomer (SYLGARD® 184; Dow Corning). A sufficient quantity of Ham's F10 Nutrient Mix (Invitrogen, UK) was added to keep the tissue moist but not submerged. For SPIM imaging, UVJ folds were cut individually with iris scissors and mounted one at a time, on a custom-made sample holder (see Supplementary Material) using fine insect needles. The sample holder, with the UVJ fold mounted, was immersed in phenol-free DMEM/F12 media, at 37º C during imaging.

SPIM imaging

155 Live UVJ tissue samples, prepared as above, were imaged using a custom-built SPIM
156 microscope (at the University of Sheffield) with laser excitation at 473 nm and a 520
157 nm long pass (LP) fluorescence emission filter (Semrock, Inc.). The microscope
158 hardware and optical components was based on the OpenSPIM platform (58) but
159 with modifications detailed in Mendonca *et al.* [59; supplementary materials]. The
160 camera, detection and illumination objectives, and magnification were fixed for the
161 system, ensuring that the imaging results were reproduceable. The autofluorescence
162 image stacks were acquired using 500 ms exposure, starting at the outer surface and
163 moving up to 100 μm deep into the tissue fold.
164
165 *Characterisation of autofluorescence*
166 SSTs were clearly identifiable in live UVJ tissue during fluorescence imaging on the
167 SPIM and had a punctate appearance on account of autofluorescent granules (Figure
168 1) which appeared to be mostly confined to SST epithelial cells and were present
169 along the entire length of the SST from orifice to blind end. No other cell structure or
170 organelle was visible in these autofluorescence images.
171
172 To determine the organisation of the autofluorescent granules in the SST epithelium,
173 label-free images from live UVJ folds (n = 10 birds) were compared to those of fixed
174 UVJ folds that had been stained for nucleic acids (n = 3 birds). Folds were also
175 examined on a bright-field microscope after histological sectioning and general
176 histochemical staining (n = 3 birds) (Supplementary Material).

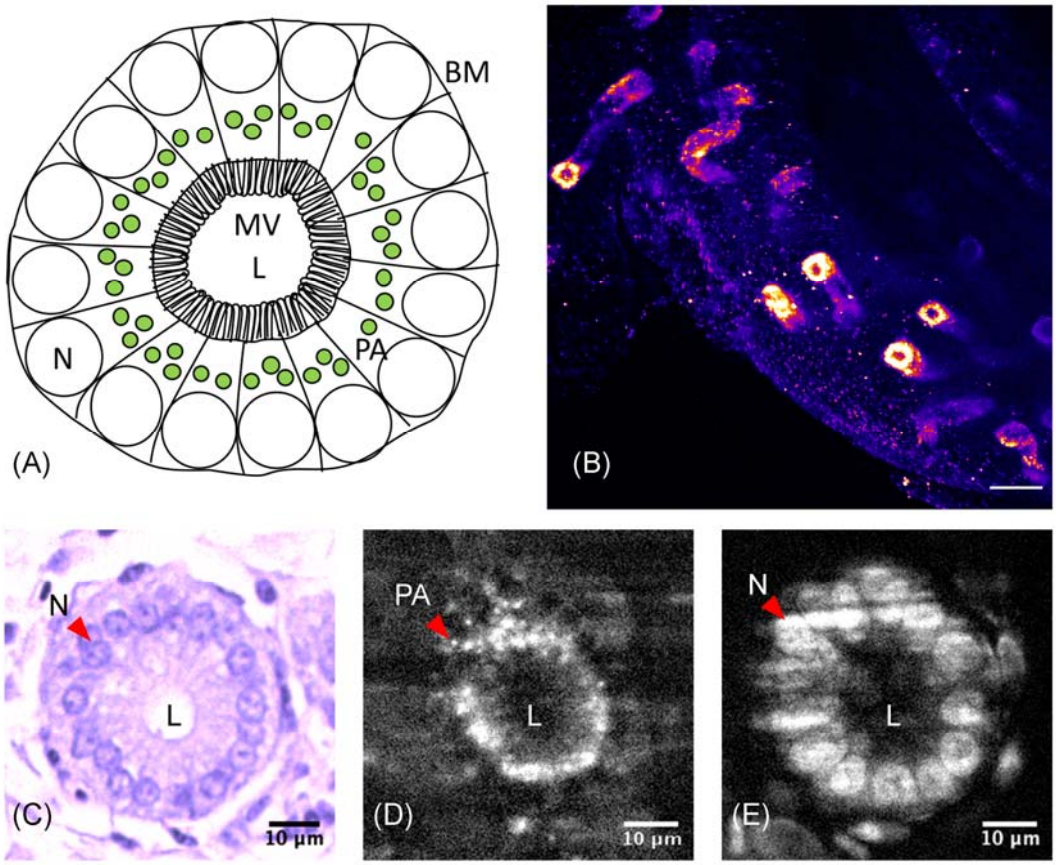

Figure 1: (A) Schematic of SST transverse section showing cellular polarisation with nuclei (N) towards the basement membrane (BM) and microvilli (MV) at the apical end of the epithelium. The punctate autofluorescence (PA) detected by the SPIM is present proximal to the nucleus but not at the apical end of the epithelium near the lumen (L). **(B)** Max intensity projection of a UVJ fold with multiple detectable SSTs imaged on the SPIM. Scale – 50 µm **(C)-(E)** Cross section of SST from histology, autofluorescence imaged on the SPIM, and SYTO-13 labelled nuclei imaged on the SPIM respectively. Scale – 10 µm.

185 *Image Analysis*

186 The image stacks acquired using the SPIM were used to reconstruct 480 μm x 480
187 μm x 100 μm tissue sections containing 3D information on SST structure (n = 10
188 females, one SST per female). SST shape information was extracted by measuring the
189 diameter enclosed by the autofluorescence from images of live tissue, at ten
190 equidistant points along the length of the SST.

191

192 UVJ tissue image stacks were first pre-processed in Fiji (60). Individual unbranched
193 SSTs were selected from each female such that the entire SST structure was included
194 in the 3D image stacks. The SSTs follow convoluted paths through the UVJ fold tissue,
195 so in order to measure cross-sectional diameter at multiple points, it was necessary
196 to slice the image volume at arbitrary angles to ensure the measurement planes
197 were perpendicular to the direction of the SST structure. This was accomplished by
198 first tracing the direction of the SST structure using a dilated version of the SST
199 image (generated using the 'MorphoLibJ' plugin (61) followed by the application of
200 Gaussian blur), to smooth the punctate autofluorescence. Two outlines for each SST
201 were then semi-automatically traced in 3D, from the orifice to the blind end and
202 along opposite sides of the SST lumen, using the 'Simple Neurite Tracer' (62) plugin
203 in Fiji.

204

205 The next stage of image analysis was performed using MATLAB® (2015b, version
206 8.6, MathWorks, Natick, MA). An average trace which passed through the SST lumen
207 was computed from the two traces for each SST. SST lengths were measured from
208 these average traces. For each SST (n = 10), the average trace was interpolated at ten
209 equidistant points (the first at the orifice and the tenth point before the blind end of

210 the tubule) and at each interpolated point a vector describing the direction of the
211 SST at that point was computed using its nearest neighbouring points on the trace
212 (Figure 2). By using these vectors and the interpolated points, slicing planes normal
213 to the vectors were defined. The indices for these slicing planes were used to extract
214 2D image sections from the un-dilated original image stacks using the
215 'ExtractSlice.m' (63) function. For every extracted slice, its distance from the orifice
216 along the luminal trace of the SST was computed using the 'Arclength.m' (64)
217 function, and the major axis diameter (d1) and the minor axis diameter (d2) of the
218 SST (enclosed by autofluorecence) were measured.

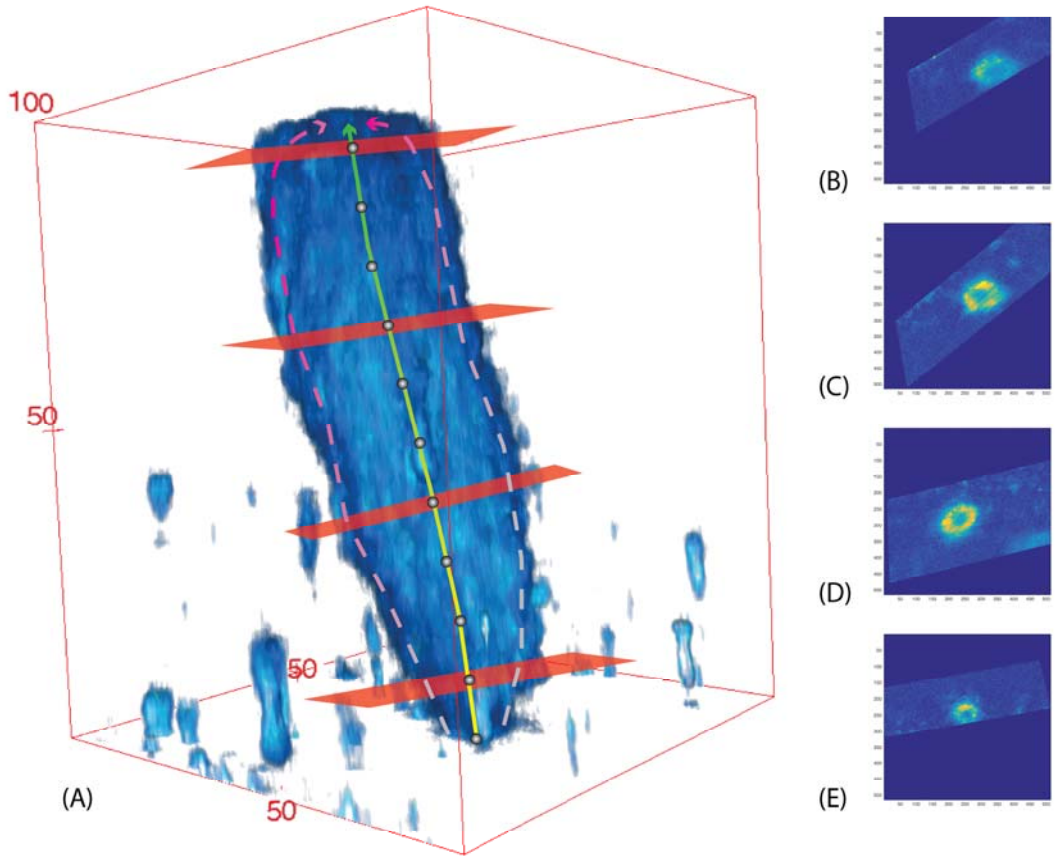

Figure 2: Illustration of the image analysis pipeline. (A) 3D rendering of an SST overlaid with traces along the sides (dotted lines), the computed trace through the centre and slices perpendicular to the direction of the SST at 4 example positions (SSTs were sampled at 10 positions represented by grey dots). **(B-E)** Corresponding slices through the SST. Measurements were taken of the major axis and minor axis diameter for each of the slices. Axis units in pixels (converted to microns before data analysis).

Statistical Analysis:

Data analysis was performed using the statistical package R, version 3.2.3 (65). We tested whether SST diameter varied with SST length using a mixed effects model ('lmer' function from the 'lme4' package (66) along with the 'lmerTest' package (67)) with average SST diameter [(d1+ d2) / 2] at the sampled point as the dependent variable, the distance of sampled point from SST orifice and the SST total length as fixed effects, and the bird ID as a random effect to account for repeated measures from each female.

We also assessed if the SST was elliptical or circular in cross-section (the former providing greater epithelial apical surface area for increased contact with sperm) and whether any such ellipticity changed in response to SST length. A circularity index was first calculated by dividing the major axis diameter (d1) by the minor axis diameter (d2), where a circularity index of one indicates a circular SST cross-section. Data were then analysed via a mixed effects model using the 'lmer' function (66), with the circularity index as the dependent variable and the total length of the SST as a fixed effect. The sum of the major and minor axis diameters (d1+ d2) was also incorporated as a fixed effect to account for magnitude of change in diameter along each axis, as well as the distance of sampled point from SST orifice, with an interaction term between them. As before, bird ID was included as a random effect to account for repeated measures from each female.

Results:

The diameter of SSTs was found to be notably constricted at their orifice, suggestive of a structural 'barrier' for entry and exit (Figure 3 (A)). Beyond this constricted

entrance, SSTs were largely tubular in shape, with diameter increasing marginally along the SST's length until its mid-point, after which diameter decreased again towards the blind end of the SST. This shape can be described by a significant quadratic relationship between SST diameter and the distance from the SST orifice (estimated effect = -16.761, t = -3.085, p = 0.003; Figure 3 (B)). The relationship between SST diameter and distance from the SST orifice was also found using data from labelled tissue (Supplementary Figure S4), confirming that the shape measured from autofluorescence images was not an artefact resulting from the distribution of the autofluorescence granules. Long SSTs were neither wider nor thinner than short SSTs (estimated effect = 0.038, t = 1.058, p = 0.319).

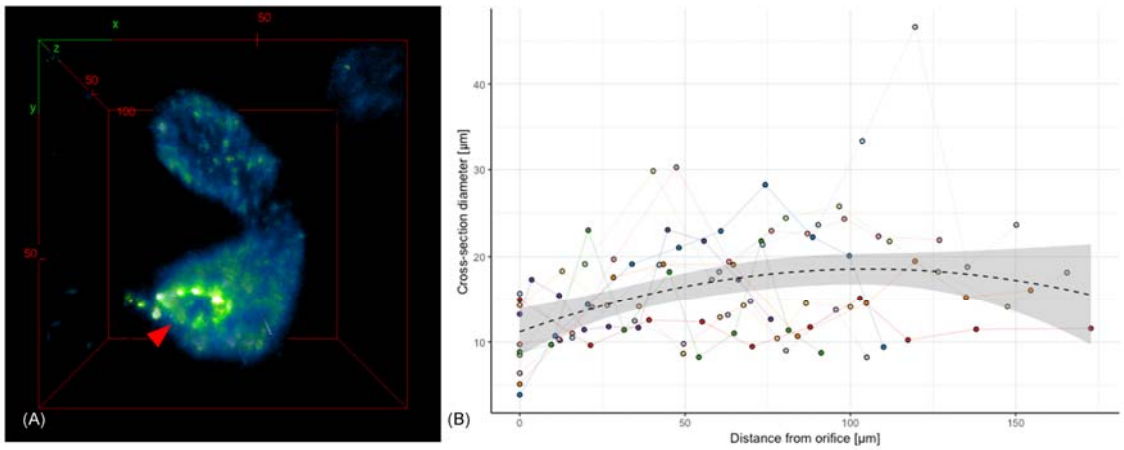

Figure 3: (A) 3D rendering of an SST showing its constricted orifice (arrowhead). **(B)** SST diameter has a quadratic relationship with distance from the SST opening suggesting a constriction at the orifice and a slight increase in diameter along its length up to the middle of the SST. Each colour on the plot represents measurements from the same SST (n = 10). Scale on red bounding box is in microns.

SSTs were found to be slightly elliptical in cross-section, with the major axis diameter being 1.642 ± 0.168 times larger than the minor axis diameter. The

circularity of the SST in cross-section did not vary significantly with SST diameter (estimated effect = 0.014, t = 0.979, p = 0.330), distance from orifice (estimated effect = 0.003, t = 0.587, p = 0.558), or the interaction between these two variables (estimated effect = -0.00009, t = -0.587, p = 0.559). Circularity was also not related to SST total length (estimated effect = -0.004, t = -1.14, p = 0.282).

Comparisons between the SST measurements from histology and SPIM images indicate that the autofluorescent granules are present in the supranuclear region of the SST epithelium (Figure 1). The size of the lumen diameter scaled linearly with the width of the SST (Supplementary Figure S4), indicating that epithelial cells remained the same thickness in cross-section with increasing SST diameter. This allowed us to extrapolate shape information from the above analyses to the SST lumen, and using this method, we estimated the diameter of the SST orifice to be 3.278 ± 1.115 µm (mean ± SD; Table 1).

	Diameter (mean ± SD)	
	at orifice (µm)	**at widest section (µm)**
inter-nuclear diameter[1]	12.060 ± 1.419	30.830 ± 11.055
autofluorescence[1]	10.065 ± 4.288	16.374 ± 6.610
lumen diameter[2]	3.278 ± 1.115	9.128 ± 1.377

Table 1: SST dimensions at orifice and widest section - SST diameter is the smallest at its orifice and widest near the middle along its length.

[1]Measurements acquired from SPIM image z-stacks

[2]SST lumen diameter values were predicted from the model describing the relationship between lumen and inter-nuclear diameter.

292 **Discussion:**

293 Using novel 3D imaging methods, we have demonstrated for the first time the
294 existence of a constricted orifice at the entrance/exit of avian SSTs. Such a structure
295 is likely to play an important role in sperm selection at storage. Zaferani *et al.* (68)
296 recently used *in vitro* techniques to demonstrate how constrictions can act as gate-
297 like selective barriers to sperm, allowing only sperm swimming above a threshold
298 velocity to overcome the shear rate at the constriction and pass through. The narrow
299 SST orifices we have found have a mean diameter of ~3 μm; this, with the added
300 obstruction of microvilli (1-2 μm in length (52)), must act to restrict the rate of
301 sperm (mean diameter at mid-piece - ~0.6 μm (59)) entering and exiting the SST. We
302 therefore propose that the constricted opening we have found in SST tubules
303 provides a mechanism by which sperm storage and release can be regulated. This
304 supports the idea that avian SSTs play an active and selective role in sperm storage,
305 regulating sperm uptake and release (33–38). The constricted orifice, together with
306 its microvilli, may act as a valve, enforcing unidirectional movement of sperm and
307 preventing them from being flushed back out. The small luminal diameter along the
308 SST (mean: 9 μm, Table 1) may also limit the ability of sperm to turn around inside
309 the SST and swim out.

310

311 In terms of overall structure, we found SSTs to be slightly elliptical in cross-section,
312 with the major axis diameter being about 1.6 times larger than the minor axis
313 diameter. This ellipticity was independent of SST radius, the distance along the SST
314 from orifice, or total SST length. Cross-sectional ellipticity increases the surface area
315 of the SST epithelial apical surface, allowing for a greater number of microvilli (as

316 compared to a circular lumen with the same volume) for increased contact with
317 sperm and optimum exchange of nutrients and waste.
318
319 We found SST diameter to vary widely across zebra finch SSTs. Birkhead *et al.* (69)
320 suggested that some SSTs might remain inactive in the zebra finch UVJ, even in its
321 fully developed state. It is possible that some of the variation in SST shape that we
322 observed can be explained by the presence of functional and non-functional SSTs,
323 but it is unclear whether thinner, more uniform SSTs, or more distended morphs
324 would represent the active state. Mero and Ogasawara (70), and Burke (71)
325 described 'swollen' tubules in chickens and suggested swelling to be associated with
326 sperm release. Such swellings might help explain the outliers in our data (Figure 3
327 (B)). It is possible that conformational changes in SST shape from functional to non-
328 functional states may be enabled by the F-actin rich terminal web, as seen in turkey
329 SSTs (39), and caused by neural stimulation (39, 72) and/or hormonal effects (48,
330 49). Variation in SST shape might also be explained by factors not tested in this
331 study, including age, hormone levels and location of the SST in the UVJ.
332
333 About 4 – 27% of all the sperm storage tubules in the zebra finch UVJ are branched
334 (28, 73). Branched tubules were not included in our study, but individual branches
335 are expected to show similar shapes as unbranched tubules. Hemmings and
336 Birkhead (28) described sperm from different males differentially stored in separate
337 branches of an SST (albeit a single observation, since in most cases sperm from
338 different males were stored in different SSTs). Further study of the 3D structure of
339 branched SSTs could shed light on mechanisms that prevent sperm mixing in
340 branched tubules.

341

342 Our novel 3D data on SST structure were made possible by the presence of
343 punctate/granular autofluorescence, confined to the SST epithelial cells and
344 uniformly distributed throughout the SST's entire length. These granules were found
345 to have a supranuclear localisation in the SST epithelial cells (Figure 1). Although
346 identifying the exact source of the autofluorescence was beyond the scope of this
347 study, autofluorescence in a similar range has been noted in the ewe (*Ovis aries*)
348 endometrium ($\lambda_{ex}/\lambda_{em}$ = 488/525-575 nm) (74) and in human colonic crypts ($\lambda_{ex}/\lambda_{em}$
349 = 488/580 nm) (75). While such autofluorescence has been attributed to NADH
350 metabolism in mitochondria (74, 76), another likely source might be lipofuscin in
351 lysosomes (75). Mitochondria are not confined to the apical cytoplasm of SST
352 epithelium as observed in turkeys (77) and chickens (78), so it is unlikely that these
353 granules represent mitochondria. Lysosomes on the other hand, are globular
354 vesicles similar in size (< 1 μm) to the autofluorescent granules observed here (79),
355 and have been detected in the apical cytoplasm of turkey SST epithelia (77), and less
356 abundantly in chickens (78) and passerine alpine accentor (*Prunella collaris*) (79).
357 Multiple studies have also detected the presence of acid phosphatase, an enzyme
358 found in lysosomes, in the supranuclear cytoplasm of SST epithelia in turkeys (21),
359 quail (80), chickens, (81) and ducks (*Anas sp.*) (82), but not in the SST lumen, which
360 corresponds with the autofluorescence pattern we observed here in the zebra finch.
361 Acid phosphatase has been implicated in autolysis associated with oviduct
362 regression (83) as well as with sperm release (82). If this is true, the label-free
363 imaging methods developed here may provide exciting new means for investigating
364 SST functional development throughout the reproductive cycle. Identifying the

chemical nature of the autofluorescent substance present in SST granules therefore represents an important avenue for future research.

In summary, we have demonstrated that sperm storage structures in living vertebrate oviductal tissue can be imaged label-free using SPIM microscopy, and this novel 3D imaging technique has enabled us to produce the most detailed account of avian SST structure to date, including the discovery of a previously undescribed gate-like constriction at the entrance/exit of tubules that is likely to act as a key selective barrier. The imaging methods described here hold immense potential for studying *in vivo* sperm storage and sperm-female interactions.

Authors' contributions:

T.M. coordinated the study, conducted the experiments and analyses, and wrote the manuscript; N.H. conceived the study, conducted the sperm motility experiment and advised on data analyses. All authors participated in the design of the study, helped draft the manuscript and gave final approval for publication.

Acknowledgements:

The authors are grateful to Prof Tim Birkhead and Prof Simon Jones from the University of Sheffield for support. Thanks to Mark Kinch from Skelet.AL, Phil Young, Lynsey Gregory, Emily Glendenning and Jamie Thompson from the University of Sheffield for technical assistance.

References:

1. Birkhead, T.R. 1992. Sperm Storage and the Fertile Period in the Bengalese Finch.

390 Auk. 109: 620–625.
391 2. Birkhead, T.R., and A.P. Møller. 1995. Extra-pair copulation and extra-pair
392 paternity in birds. Anim. Behav. 49: 843–848.
393 3. Hanken, J., and P.W. Sherman. 1981. Multiple paternity in Belding's ground
394 squirrel litters. Science (80-.). 212: 351–353.
395 4. Tegelström, H., J. Searle, J. Brookfield, and S. Mercer. 1991. Multiple paternity in
396 wild common shrews (Sorex araneus) is confirmed by DNA-fingerprinting.
397 Heredity (Edinb). 66 (Pt 3): 373–379.
398 5. Amos, W., S. Twiss, P.P. Pomeroy, and S.S. Anderson. 1993. Male mating success
399 and paternity in the grey seal, Halichoerus grypus: a study using DNA
400 fingerprinting. Proc. R. Soc. B. 252: 199–207.
401 6. Uller, T., and M. Olsson. 2008. Multiple paternity in reptiles: Patterns and
402 processes. Mol. Ecol. 17: 2566–2580.
403 7. Avise, J.C., A.G. Jones, D. Walker, and J.A. DeWoody. 2002. Genetic mating systems
404 and reproductive natural histories of fishes: lessons for ecology and evolution.
405 Annu. Rev. Genet. 36: 19–45.
406 8. Gromko, M.H., D.G. Gilbert, and R.C. Richmond. 1984. Sperm transfer and use in
407 the multiple mating system of Drosophila. Sperm Compet. Evol. Anim. mating
408 Syst. : 371–426.
409 9. Moritz, R.F.A., P. Kryger, G. Koeniger, N. Koeniger, A. Estoup, and S. Tingek. 1995.
410 High degree of polyandry in Apis dorsata queens detected by DNA microsatellite
411 variability. Behav. Ecol. Sociobiol. 37: 357–363.
412 10. Crozier, R.H., and E.J. Fjerdingstad. 2001. Polyandry in social Hymenoptera -
413 disunity in diversity? Ann. Zool. Fennici. 38: 267–285.
414 11. Birkhead, T.R., and A.P. Møller. 1998. Sperm competition and sexual selection.

415 Academic Press.
416 12. Simmons, L.W. 2001. Sperm competition and its evolutionary consequences in the
417 insects. Princeton University Press.
418 13. Eberhard, W.G. 1996. Female Control: Sexual Selection by Cryptic Female Choice.
419 Princeton University Press.
420 14. Córdoba-Aguilar, A., E. Uhía, and A.C. Rivera. 2003. Sperm competition in Odonata
421 (Insecta): the evolution of female sperm storage and rivals' sperm displacement.
422 J. Zool. 261: 381–398.
423 15. Siva-Jothy, M.T. 1987. The structure and function of the female sperm-storage
424 organs in libellulid dragonflins. J. Insect Physiol. 33: 559–567.
425 16. Ward, P.I. 1993. Females influence sperm storage and use in the yellow dung fly
426 Scathophaga stercoraria (L.). Behav. Ecol. Sociobiol. 32.
427 17. Pitnick, S., T. Markow, and G.S. Spicer. 1999. Evolution of Multiple Kinds of Female
428 Sperm-Storage Organs in Drosophila. Evolution (N. Y). 53: 1804.
429 18. Fox, W. 1956. Seminal receptacles of snakes. Anat. Rec. 124: 519–539.
430 19. Conner, J., and D. Crews. 1980. Sperm transfer and storage in the lizard Anolis
431 carolinensis. J. Morphol. 163: 331–348.
432 20. Gist, D.H., and J.M. Jones. 1989. Sperm storage within the oviduct of turtles. J.
433 Morphol. 199: 379–384.
434 21. Zavaleta, D., and F. Ogasawara. 1973. A review of the mechanism of the release of
435 spermatozoa from storage tubules in the fowl and turkey oviduct. Worlds. Poult.
436 Sci. J. 43: 132–139.
437 22. Bakst, M.R. 1987. Anatomical basis of sperm-storage in the avian oviduct.
438 Scanning Microsc. 1: 1257.
439 23. Bobr, L.W., F.W. Lorenz, and F.X. Ogasawara. 1964. Distribution of Spermatozoa in

440 the Oviduct and Fertility in Domestic Birds. I. Residence Sites of Spermatozoa in
441 Fowl Oviducts. J. Reprod. Fertil. 8: 39–47.
442 24. Birkhead, T.R., and A.P. Møller. 1992. Numbers and size of sperm storage tubules
443 and the duration of sperm storage in birds: a comparative study. Biol. J. Linn. Soc.
444 45: 363–372.
445 25. Steele, M.G., and G.J. Wishart. 1996. Demonstration that the removal of sialic acid
446 from the surface of chicken spermatozoa impedes their transvaginal migration.
447 Theriogenology. 46: 1037–1044.
448 26. King, L.M., J.P. Brillard, W.M. Garrett, M.R. Bakst, and A.M. Donoghue. 2002.
449 Segregation of spermatozoa within sperm storage tubules of fowl and turkey
450 hens. Reproduction. 123: 79–86.
451 27. Briskie, J. V. 1996. Spatiotemporal patterns of sperm storage and last-male sperm
452 precedence in birds. Funct. Ecol. 10: 375–383.
453 28. Hemmings, N., and T.R. Birkhead. 2017. Differential sperm storage by female
454 zebra finches Taeniopygia guttata. Proc. R. Soc. B. 284: 20171032.
455 29. Froman, D.P. 2003. Deduction of a model for sperm storage in the oviduct of the
456 domestic fowl (Gallus domesticus). Biol. Reprod. 69: 248–53.
457 30. Froman, D.P., T. Pizzari, A.J. Feltmann, H. Castillo-Juarez, and T.R. Birkhead. 2002.
458 Sperm mobility: mechanisms of fertilizing efficiency, genetic variation and
459 phenotypic relationship with male status in the domestic fowl, Gallus gallus
460 domesticus. Proc. R. Soc. B. 269: 607–12.
461 31. Birkhead, T.R., J.E. Pellatt, and F.M. Hunter. 1988. Extra-pair copulation and sperm
462 competition in the zebra finch. Nature. 334: 60–2.
463 32. Birkhead, T.R., and J.D. Biggins. 1998. Sperm competition mechanisms in birds:
464 models and data. Behav. Ecol. 9: 253–260.

465 33. Matsuzaki, M., S. Mizushima, G. Hiyama, N. Hirohashi, K. Shiba, K. Inaba, T. Suzuki,
466 H. Dohra, T. Ohnishi, Y. Sato, T. Kohsaka, Y. Ichikawa, Y. Atsumi, T. Yoshimura, and
467 T. Sasanami. 2015. Lactic acid is a sperm motility inactivation factor in the sperm
468 storage tubules. Sci. Rep. 5: 17643.
469 34. Holm, L., H. Ekwall, G.J. Wishart, Y. Ridderstråle, and Y. Ridderstrale. 2000.
470 Localization of calcium and zinc in the sperm storage tubules of chicken, quail and
471 turkey using X-ray microanalysis. J. Reprod. Fertil. 118: 331–336.
472 35. Bakst, M.R., and M.P. Richards. 1985. Concentrations of selected cations in turkey
473 serum and oviductal mucosae. Poult. Sci. 64: 555–563.
474 36. Holm, L., and Y. Ridderstråle. 1998. Localization of carbonic anhydrase in the
475 sperm-storing regions of the turkey and quail oviduct. Histochem. J. 30: 481–488.
476 37. Holm, L., and G.J. Wishart. 1998. The effect of pH on the motility of spermatozoa
477 from chicken, turkey and quail. Anim. Reprod. Sci. 54: 45–54.
478 38. Holm, L., S.D. Ruziwa, V. Dantzer, and Y. Ridderstråle. 2000. Carbonic anhydrase
479 in the utero-vaginal junction of immature and mature ostriches. Br. Poult. Sci. 41:
480 244–9.
481 39. Freedman, S.L., V.G. Akuffo, and M.R. Bakst. 2001. Evidence for the innervation of
482 sperm storage tubules in the oviduct of the turkey (Meleagris gallopavo).
483 Reproduction. 121: 809–814.
484 40. Atherton, R.W., C.M. Cisson, B.W. Wilson, and T.K. Golder. 1980. Quantitation of
485 avian spermatozoan motility: Neurochemical regulation. Gamete Res. 3: 17–24.
486 41. Hiyama, G., M. Matsuzaki, S. Mizushima, H. Dohra, K. Ikegami, T. Yoshimura, K.
487 Shiba, K. Inaba, and T. Sasanami. 2014. Sperm activation by heat shock protein 70
488 supports the migration of sperm released from sperm storage tubules in Japanese
489 quail (Coturnix japonica). Reproduction. 147: 167–178.

490 42. Lindquist, S., and E.A. Craig. 1988. the Heat -Shock Proteins. Annu. Rev. Genet. 22:
491 631–677.
492 43. Van Krey, H.P., F.X. Ogasawara, and J. Pangborn. 1967. Light and Electron
493 Microscopic Studies of Possible Sperm Gland Emptying Mechanisms. Poult. Sci.
494 46: 69–78.
495 44. Gilbert, A.B., M.E. Reynolds, and F.W. Lorenz. 1968. Distribution of spermatozoa in
496 the oviduct and fertility in domestic birds. V. Histochemistry of the uterovaginal
497 sperm-host glands of the domestic hen. J. Reprod. Fertil. 16: 433–44.
498 45. Hirokawa, N., T.C.S. Keller, R. Chasan, and M.S. Mooseker. 1983. Mechanism of
499 brush border contractility studied by the quick-freeze, deep-etch method. J. Cell
500 Biol. 96: 1325–1336.
501 46. Keller, T.C.S., K.A. Conzelman, R. Chasan, and M.S. Mooseker. 1985. Role of myosin
502 in terminal web contraction in isolated intestinal epithelial brush borders. J. Cell
503 Biol. 100: 1647–1655.
504 47. Owaribe, K., R. Kodama, and G. Eguchi. 1981. Demonstration of contractility of
505 circumferential actin bundles and its morphogenetic significance in pigmented
506 epithelium in vitro and in vivo. J. Cell Biol. 90: 507–514.
507 48. Ito, T., N. Yoshizaki, T. Tokumoto, H. Ono, T. Yoshimura, A. Tsukada, N. Kansaku,
508 and T. Sasanami. 2011. Progesterone is a sperm-releasing factor from the sperm-
509 storage tubules in birds. Endocrinology. 152: 3952–3962.
510 49. Hemmings, N., T.R. Birkhead, J.P. Brillard, P. Froment, and S. Briere. 2015. Timing
511 associated with oviductal sperm storage and release after artificial insemination
512 in domestic hens. Theriogenology. 83: 1174–1178.
513 50. Bakst, M.R. 1998. Structure of the avian oviduct with emphasis on sperm storage
514 in poultry. J. Exp. Zool. 282: 618–626.

515 51. Van Drimmelen, G.C. 1946. “Spermnests” in the oviduct of the domestic hen. J.
516 South African Vet. Med. Assoc. 17: 42–52.
517 52. Bakst, M.R., and G. Bauchan. 2015. Apical blebs on sperm storage tubule epithelial
518 cell microvilli: Their release and interaction with resident sperm in the turkey
519 hen oviduct. Theriogenology. 83: 1438–44.
520 53. Bakst, M.R. 1992. Observations on the turkey oviductal sperm-storage tubule
521 using differential interference contrast microscopy. J. Reprod. Fertil. 95: 877–883.
522 54. Huisken, J., J. Swoger, F. Del Bene, J. Wittbrodt, and E.H.K. Stelzer. 2004. Optical
523 Sectioning Deep Inside Live Embryos by Selective Plane Illumination Microscopy.
524 Science (80-.). 305: 1007–1009.
525 55. Reynaud, E.G., U. Krzic, K. Greger, and E.H.K. Stelzer. 2008. Light sheet-based
526 fluorescence microscopy: more dimensions, more photons, and less
527 photodamage. HFSP J. 2: 266–75.
528 56. Birkhead, T.R., J.E. Pellatt, P. Brekke, R. Yeates, and H. Castillo-Juarez. 2005.
529 Genetic effects on sperm design in the zebra finch. Nature. 434: 383–7.
530 57. Bennison, C., N. Hemmings, J. Slate, and T. Birkhead. 2015. Long sperm fertilize
531 more eggs in a bird. Proc. R. Soc. B. 282: 20141897.
532 58. Pitrone, P.G., J. Schindelin, L. Stuyvenberg, S. Preibisch, M. Weber, K.W. Eliceiri, J.
533 Huisken, and P. Tomancak. 2013. OpenSPIM: an open-access light-sheet
534 microscopy platform. Nat. Methods. 10: 598–599.
535 59. Mendonca, T., T.R. Birkhead, A.J. Cadby, W. Forstmeier, and N. Hemmings. 2018. A
536 trade-off between thickness and length in the zebra finch sperm mid-piece. Proc.
537 R. Soc. B Biol. Sci. 285: 20180865.
538 60. Schindelin, J., I. Arganda-Carreras, E. Frise, V. Kaynig, M. Longair, T. Pietzsch, S.
539 Preibisch, C. Rueden, S. Saalfeld, B. Schmid, J.-Y. Tinevez, D.J. White, V.

Hartenstein, K. Eliceiri, P. Tomancak, and A. Cardona. 2012. Fiji: an open-source platform for biological-image analysis. Nat. Methods. 9: 676–82.

61. Legland, D., I. Arganda-Carreras, and P. Andrey. 2016. MorphoLibJ: integrated library and plugins for mathematical morphology with ImageJ. Bioinformatics. 32: 3532–3534.

62. Longair, M.H., D.A. Baker, and J.D. Armstrong. 2011. Simple neurite tracer: Open source software for reconstruction, visualization and analysis of neuronal processes. Bioinformatics. 27: 2453–2454.

63. Teng, P. 2011. Extract Slice from Volume. .

64. D'Errico, J. 2012. arclength. .

65. R Development Core Team. 2015. R: A Language and Environment for Statistical Computing. R Foundation for Statistical Computing, Vienna, Austria.

66. Bates, D.M., M. Machler, B.M. Bolker, and S.C. Walker. 2014. Fitting Linear Mixed-Effects Models using lme4. J. Stat. Softw. 67: 1--48.

67. Kuznetsova, A., P.B. Brockhoff, and R.H.B. Christensen. 2017. lmerTest Package: Tests in Linear Mixed Effects Models. J. Stat. Softw. 82: 1–26.

68. Zaferani, M., G.D. Palermo, and A. Abbaspourrad. 2019. Strictures of a microchannel impose fierce competition to select for highly motile sperm. Sci. Adv. 5: eaav2111.

69. Birkhead, T.R., J.E. Pellatt, and F.M. Hunter. 1990. Numbers and Distribution of Sperm in the Uterovaginal Sperm Storage Tubules of the Zebra Finch. Condor. 92: 508–516.

70. Mero, K.N., and F.X. Ogasawara. 1970. Dimensions of uterovaginal sperm-storage tubules of the chicken and their possible significance in sperm release. Poult. Sci. 49: 1304–1308.

565 71. Burke, W.H. 1968. Release of spermatozoa from storage sites in the hen's oviduct.
566 .
567 72. Gilbert, A.B., and P.E. Lake. 1963. Terminal Innervation of the Uterus and Vagina
568 of the Domestic Hen. Reproduction. 5: 41–NP.
569 73. Birkhead, T.R., and F.M. Hunter. 1990. Numbers of sperm-storage tubules in the
570 Zebra Finch (Poephila guttata) and Bengalese Finch (Lonchura striata). Auk. 107:
571 193–197.
572 74. Druart, X., J. Cognié, G. Baril, F. Clément, J.L. Dacheux, J.L. Gatti, J. Cognie, G. Baril, F.
573 Clement, J.L. Dacheux, and J.L. Gatti. 2009. In vivo imaging of in situ motility of
574 fresh and liquid stored ram spermatozoa in the ewe genital tract. Reproduction.
575 138: 45–53.
576 75. DaCosta, R.S. 2005. Autofluorescence characterisation of isolated whole crypts
577 and primary cultured human epithelial cells from normal, hyperplastic, and
578 adenomatous colonic mucosa. J. Clin. Pathol. 58: 766–774.
579 76. Brookner, C.K., M. Follen, I. Boiko, J. Galvan, S. Thomsen, A. Malpica, S. Suzuki, R.
580 Lotan, and R. Richards-Kortum. 2000. Autofluorescence Patterns in Short-term
581 Cultures of Normal Cervical Tissue. Photochem. Photobiol. 71: 730–736.
582 77. Schuppin, G.T., H.P. Van Krey, D.M. Denbow, M.R. Bakst, and G.B. Meyer. 1984.
583 Ultrastructural analyses of uterovaginal sperm storage glands in fertile and
584 infertile turkey breeder hens. Poult Sci. 63: 1872–1882.
585 78. Burke, W.H., F.X. Ogasawara, and C.L. Fuqua. 1972. A study of the ultrastructure of
586 the uterovaginal sperm-storage glands of the hen, Gallus domesticus, in relation
587 to a mechanism for the release of spermatozoa. J. Reprod. Fertil. 29: 29–36.
588 79. Chiba, A., and M. Nakamura. 2001. Microscopic structure of the sperm storage
589 tubules in the polygynandrous alpine accentor, Prunella collaris (Aves). Acta Zool.

590 82: 299–306.

591 80. Renden, J.A., E.B. May, and F.H. Benoff. 1981. Histochemistry of uterovaginal
592 sperm-host glands in Japanese Quail (Coturnix coturnix japonica) with reference
593 to the period of oviposition. Poult. Sci. 60: 2529–2535.

594 81. Gilbert, A.B., M.E. Reynolds, and F.W. Lorenz. 1968. Distribution of spermatozoa in
595 the oviduct and fertility in domestic birds. 8. The effect of a foreign object in the
596 uterus on secretions of the sperm-host glands and the survival of spermatozoa in
597 the oviduct of the domestic hen. J. Reprod. Fertil. 17: 311–4.

598 82. Pal, D. 1977. Histochemistry of the utero-vaginal junction with special reference
599 to the sperm-host glands in the oviduct of the domestic duck. Folia Histochem.
600 Cytochem. (Krakow). 15: 235–42.

601 83. Heryanto, B., Y. Yoshimura, T. Tamura, and T. Okamoto. 1997. Involvement of
602 Apoptosis and Lysosomal Hydrolase Activity in the Oviducal Regression During
603 Induced Molting in Chickens: A Cytochemical Study for End Labeling of
604 Fragmented DNA and Acid Phosphatase Treatment of Birds and Collection of
605 Samples. Poult. Sci. 76: 67–72.

606